Proceedings of HBSM 2009

Fabrication, characterization and its local reflection properties of a metal-mirror microcavity with high concentrated PIC J-aggregates

Masaru Oda[a,b,] *, Yuki Obara[b], Keita Saito[b], Kohei Higashi[b], and Toshiro Tani[a,b]

[a] *Institute of Symbiotic Science and Technology,*
[b] *Department of Applied Physics,*
Tokyo University of Agriculture and Technology, Naka-cho 2-24-16, Kogane-i, Tokyo 184-8588, Japan

Abstract

We have investigated reflection properties of light-matter strong coupling in a planar metal-mirror microcavity with highly concentrated PIC J-aggregates. Large vacuum Rabi-splitting ranging from 100 to 250 meV is obtained depending on the concentration of the J-aggregates. The factors for providing these large Rabi-splitting will be discussed based on its concentration dependence. We also present our recent study focused on microscopic reflection properties of the microcavity. We have improved microscope optics which enables us to measure local reflection spectra within 0.3-µm-diameter area. Observation of incident-light-angle dependence becomes possible. We found existence of micrometer-scale inhomogeneity in the Rabi-splitting (e.g. ±10% in a 17 µm × 17 µm region), which will be interpreted mainly by the spatial distribution of J's in the active layer.
© 2010 Elsevier B.V.

1. Introduction

In the last decade, strong light-matter coupling in semiconductor microcavities has been studied extensively not only due to fundamental interest in science [1] but also to its potential applications, e.g. for zero-threshold lasers [2], light-emitting diodes (LEDs) [3] and for generator of correlated photon-pairs [4,5], as well. Among various kinds of microcavities, planar microcavities with organic semiconductors [6-8] have received considerable attention because strong coupling regime can be achieved even at room temperature. This is surely attributable to large oscillator strength of Frenkel excitons in organic materials.

Hobson et al. [9] reported that Rabi-splitting, which is an indicator of coupling strength between photon and exciton states, in a metal-metal mirror microcavity with organic materials is larger by a factor of 2.3 than that of a metal-DBR (distributed Bragg reflector) hybrid microcavity. The enhanced Rabi-splitting arises from a strong confinement effect of light by metallic mirrors [9], some of which is also discussed in the following. Large Rabi-

---

* Corresponding author. Tel.: +81-42-388-7428; fax: +81-42-385-6255.
E-mail address: odamasa@cc.tuat.ac.jp

splitting in the metal-mirror microcavities is quite fascinating for developing polariton devices such as LEDs and photon generators, even though they seems to be unsuitable for laser applications.

We have been fabricating metal-mirror microcavity structures with J-aggregates in their active layers and investigating the features on the strong light-matter coupling [10]. Recently, large Rabi-splitting up to 250 meV has been attained with highly concentrated J-aggregates. In this paper, we present at first some of the fabrication of microcavity structures and then characterize its reflection properties. Rabi-splitting depends strongly on J's concentration. We will describe the concentration dependence of Rabi-splitting a bit in detail.

To get further insight into J's optical properties due to strong coupling, we also have been investigating microscopic reflection properties. We have improved the illumination optics for the microscopic observations and some distinctive results are obtained, which will also be introduced briefly.

2. Samples and Experiments

We use J-aggregates of pseudoisocyanine dyes (PIC, Hayashibara Biochemical Laboratories Inc.) as an active medium in the organic microcavity. The chemical structure of PIC dye is shown in the inset of Fig. 1(a). PIC dye is one of the most well-known species for its remarkable formation of J-aggregates. Broken and solid lines in Fig. 1(a) show absorption spectra of PIC monomers and its J-aggregates, respectively, in methanol solutions. There appears a strong and narrow band (J-band) at 2.16eV due to the formation of J-aggregates; which can be understood with a linear Frenkel exciton picture [11-13].

Fig. 1(b) shows a schematic diagram of the microcavity structure used in this study. The cavity length is designed for $\lambda/2$ mode. Its fabrication procedure is as follows. First, aqueous solution of potassium polyvinyl sulfate (PVS) is prepared by dissolving PVS into distilled water at 90 °C. Separately, PIC dye is dissolved in methanol. Then, the PIC methanol solution is injected into the PVS aqueous solution kept at 90 °C. The resulting solution is spin-coated onto a silver evaporated silica glass substrate surface. To form a flat layer, the substrate is placed at off-centered position from rotation axis, and the spin-coating is performed by using a two-step process. Rotational speeds of the two steps are 600 rpm for 5 s and 3000 rpm for 30 s, respectively. Finally, a second silver layer is deposited onto the J-doped polymer layer by thermal evaporation.

We prepared three kinds of sample with different concentration of the J-aggregates. PIC concentrations ($[M]_{PIC}$) of the spin-casting solutions were 0.36, 0.54 and 0.72 mg/mL, respectively. PVS concentrations ($[M]_{PVS}$) of the corresponding solutions were 22, 26 and 26 mg/mL, respectively. It is noted that methanol solution turns into a gel if PIC concentration is over ca. 0.5 mg/mL, so we must optimize PVS concentrations for each PIC concentration to get the appropriate layer thickness. In order to estimate the optical density of each active layer, we prepared reference samples on the glass substrates simultaneously by using the same spin-coat solutions. The thickness of the reference layers were confirmed almost equal to that of the active layers of the corresponding microcavities, which ensures that the optical density of the active layers can be monitored by that of the reference samples.
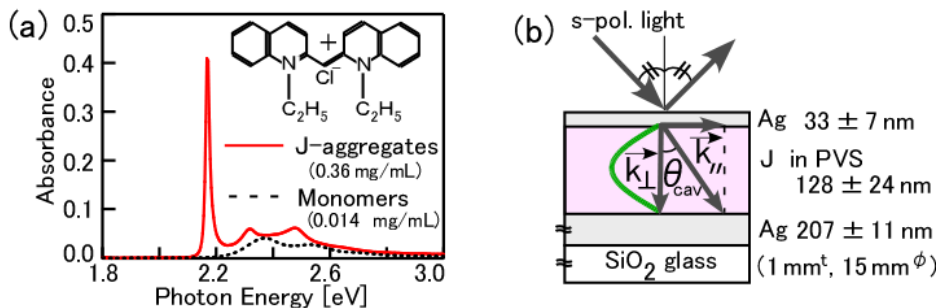

Fig. 1. (a) Absorption spectra of PIC dye monomers (dotted line) and PIC J-aggregates (solid line) dispersed in methanol at room temperature. The inset shows the chemical structure of the PIC dye molecule. (b) Schematic diagram of the $\lambda/2$-microcavity structure. The thicknesses of each layer were measured with a mechanical profilemeter (Veeco; Dectak II). Thickness and diameter of the silica glass substrate is 1 mm and 15 mm, respectively.

To measure angle-resolved reflection spectra, we prepared two optical systems, one for macroscopic and the other for microscopic observation. Figure 2(a) shows a schematic diagram of the system for the macro-observation (spatial res.; 800 μm). Light from a tungsten lamp is illuminated onto the microcavity through our fiber optics. Surface of the microcavity is sufficiently flat, so that the most of the illuminated light is reflected with the angle α according to the reflection principle. The reflected light from the active medium should be again collected by the fiber optics and detected with CCD spectroscopic detector (PI Inc.; LN/CCD) through the monochromator (ARC; SP 300-i).

Figures 2(b) and (c) show illumination and imaging optics, respectively, which are realized by our improved total internal reflection fluorescence optics combined with ordinary microscope (Nikon; TE-2000U). Spatial resolution of this system is about 0.3 μm in diameter. We describe operating principle of the microscope briefly. Monochromatic light is introduced into the microscope as incident light. To provide collimated incident light at the sample, the beam is once focused on the back focal plane (broken line B in Fig. 2(b)) of the objective lens. Incident angle α is a function of the distance from the focus spot to the optic axis of the microscope. Thus by tuning a position of the focus spot on the back focal plane we can scan the incident-angle at the sample surface. Each reflection image of specified wavelength is acquired with a 2D-CCD detector (RS; Cascade-512B) placed on the imaging plane.

As shown by grey lines in Fig. 2(c), emitted light from one local point on the sample surface is collimated by the objective and focused by the imaging lens as an imaging spot at optically corresponding location on the CCD plane. Illuminated light on the sample with incident angle α is basically reflected with reflection angle α, and can be focused as imaging spot at CCD surface. The scattered light through active sample spot, which behaves as point source of resolution size, can arrive at and be detected as the data acquisition spot at the CCD surface. Thus we can obtain local pseudo-reflection by the acquisition of photon counts within the local reflection spot ($0.3~\mu m^{\phi}$) in the image.

Local reflection spectra are reconstructed from a series of images by plotting the reflected light intensities at specific locations as a function of the wavelength. All measurements were performed at room temperature.
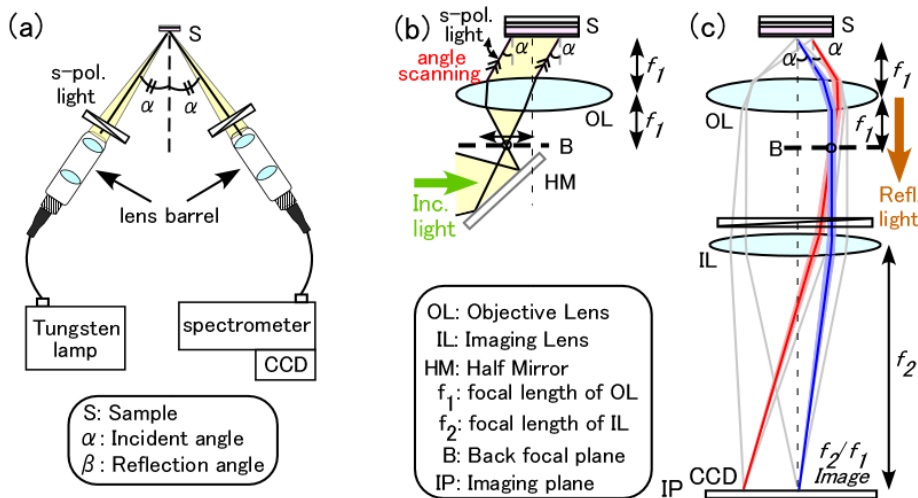

Fig. 2. (a) Optical system to measure angle-resolved reflection spectra (Spatial Res; 800 μm). By using a polarizer, linearly-polarized light perpendicular to the incident plane, i.e. s-polarized (TE) light, is illuminated to the sample. (b) and (c) show illumination and imaging optics of modified total internal reflection fluorescence microscope (Spatial Res; 0.3 μm), respectively. Likewise, s-polarized light is used for the measurements.

3. Results and Discussion

First, we characterize macroscopic reflection properties of strong light-matter coupling in the metal-mirror microcavity with high concentrated J-aggregates. Figure 3(a) shows angle-resolved reflection spectra of the sample prepared from $[M]_{PIC} = 0.54$ mg/ml solution. The spectra were measured with the macroscopic system shown in Fig.

2(a). The vertical broken line indicates the energy of Frenkel exciton of the PIC J-aggregates. Two distinctive dips ascribed as lower and upper polaritons are clearly observed in the spectra. Circles in Fig. 3(b) are the dip energies of the reflection spectra, which provides dispersion relation of cavity-polaritons in the PIC-J aggregates. Rabi-splitting of 188 meV was obtained from the best fit to the data as shown by solid lines in Fig 3(b) with an equation which derived from a coupled oscillator model [1] (see figure caption). Based on this fitting analysis, effective cavity length (L) and refractive index (n) were determined as $L_{fit} = 225 \pm 3$ nm and $n_{fit} = 1.42 \pm 0.01$ precisely.

The obtained value of L_{fit} was much larger than that of the actual thickness of the active layer (L_{active} ; 128 ± 24 nm). In order to understand this discrepancy, we evaluated at first a penetration depth of light into a metallic mirror as follows [10]. When light is reflected by a silver mirror, there appears a phase lag $\Delta\varphi$ from π in the ideal case. Thus a virtual round trip distance for the light propagation inside the mirror is $\Delta\varphi \cdot \lambda/2\pi$. It is noted that the $\Delta\varphi$ is a function of an angle θ_{cav} from the normal line of the sample surface (Fig 1(b)). The penetration depth is then estimated as $\cos\theta_{cav} \cdot \Delta\varphi \cdot \lambda/4\pi$. Effective cavity length L_{eff} ($\equiv L_{active}$ + (penetration depth of two mirrors at the resonant angle)) is estimated as 196 nm $\pm$ 36 nm and it is basically equal to L_{fit} within the error range. It is also noted that the penetration depth of silver mirrors (e.g. 68 nm; a summation of that for two mirrors) is much shorter than that of DBR mirrors (e.g. several hundreds of nanometers [1]), which is due to difference of their reflection mechanisms.

Next, we consider the n_{fit}. Experimental determination of n_{fit} can contains large ambiguity in the order of ± 0.1 easily even if the samples are fabricated under same condition simultaneously. So we consider here the average values of $n_{fit(ave)}$ for each of the concentrations. The estimated average values $n_{fit(ave)}$ were as 1.47 ± 0.1, 1.51 ± 0.1, 1.68 ± 0.1 for the samples prepared by using $[M]_{PIC} = 0.36$, 0.54 and 0.72 mg/ml solutions, respectively. At low concentrations, the $n_{fit(ave)}$ was almost equal to that of PVS matrix polymer ($n_{PVS} = 1.49$) of the active layer. Almost similar results are already reported in our previous study [10]. At higher concentration the value increases as the concentration increases. It suggests that the refractive index of the active layer is affected by the increased refractive index of PIC J-aggregates in the vicinity of the J band peak.

Thirdly, we think about the value of vacuum Rabi-splitting (Ω) using a model for planar microcavities containing quantum wells placed close to an antinode of photon electric field [14]. The model predicts that the value of Ω is
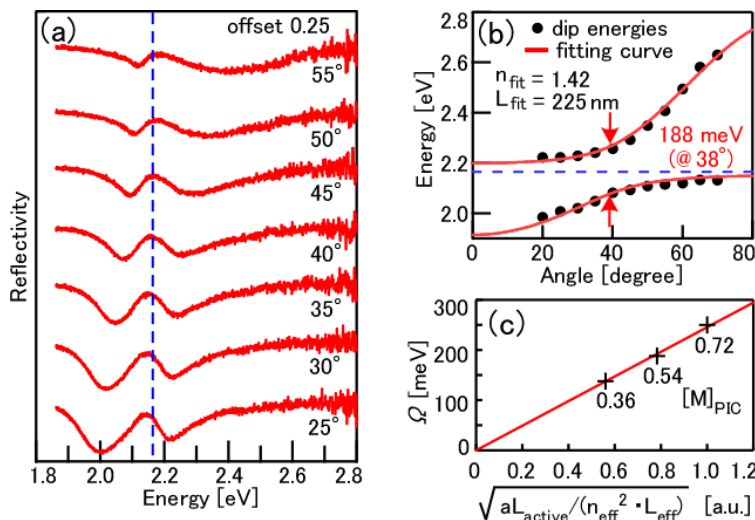

Fig. 3. (a) Reflectivity of the microcavity as a function of viewing angle for s-polarized incident light at room temperature. Viewing angles corresponding to the individual spectra are indicated on the right side. (b) Angular dependent energy dispersion of the upper and lower cavity polariton branches. The solid lines are the best fittings to the data using an equation based on a coupled oscillator model [1]. The equation is given by $E_{l,u}(\theta) = (1/2)(E_{ph}(\theta)+E_{ex}) \pm (1/2)[(E_{ph}(\theta)-E_{ex})^2+\Omega^2)]^{1/2}$, where E_{ex} (= 2.16 eV) is the exciton energy, $E_{ph}(\theta)=E_0 \times [1-(\sin\theta/n)^2]^{-1/2}$ is the energy of photon mode in the planar $\lambda/2$-microcavity and E_0 is the one at $\theta = 0$ (normal incidence). (c) The value of Ω as a function of $[\alpha L_{active}/n_{eff}^2 L_{eff}]^{1/2}$. PIC concentration associated with each point is indicated.

proportional to a factor of $(F/n^2L)^{1/2}$, where F is oscillator strength per unit area of the quantum wells. In the case of the organic microcavity, F can be replaced by a product of oscillator strength of Frenkel exciton in PIC J-aggregates and effective concentration of the J-aggregates in unit area. It is noted that the product is proportional to optical density (αL_{active}, where α is absorption coefficient) of the active layer, and can be evaluated experimentally. The Ω is therefore expected to be proportional to $(\alpha L_{active}/n_{eff}^2 L_{eff})^{1/2}$, where n_{eff} is effective refractive index in the active layer. Crosses in Fig. 3(c) show experimentally obtained Ω as a function of $(\alpha L_{active}/n_{eff}^2 L_{eff})^{1/2}$. In these plots, we used n_{fit} instead of n_{eff}. The data can be fitted quite well as a linear function, which suggests that the model is also applicable to the organic microcavity. Large Rabi-splitting ranging from 100 meV to 250 meV is obtained in the microcavity as shown in Fig 3 (c). The larger value is probably attributed to the larger oscillator strength of PIC-J excitons and actually also to high concentration of the J-aggregates. It should be noted that the shorter penetration depth of the metallic mirrors and hence smaller L_{eff} also contributes to the large Rabi-splitting [9].

To get further insight into these peculiar optical properties due to light-matter strong coupling in the microcavity, we also have been trying to extend our observations toward local regions with microscopic system shown in Figs. 2 (b) and (c), which enables us to get angle-resolved micro reflection spectra. As far as we know, this is the first report on local reflection properties in organic microcavities though it is still in its preliminary stage.

Figure 4(a) shows a microscopic reflection image of the microcavity. The sample is the same one used in the measurement shown in Fig. 3(a). This image was obtained under the condition that photon energy of the illuminated light and incident-light-angle were 2.05 eV and 18°, respectively. This, in other words, corresponds to a point on the lower polariton branch shown in Fig. 3(b). If the sample is homogenous, reflectance should be constant over the image and should be stay at low bottom intensity due to the formation of lower-polaritons. As clearly seen in the image, however, it reveals the existence of a distinctive micro-size inhomogeneity overall the image.

Figures 4(b) -A, -B and -C show angle-resolved reflection spectra, respectively, obtained at the locations indicated by squares A, B and C in Fig. 4(a). Two distinctive dips due to cavity polaritons are observed in each spectrum. It is also made clear that these dips in the microscopic spectra are narrower and deeper by a factor of 2 than those in the macroscopic spectra as shown in Fig. 4(c). Sharpening of the microscopic spectra indicates that
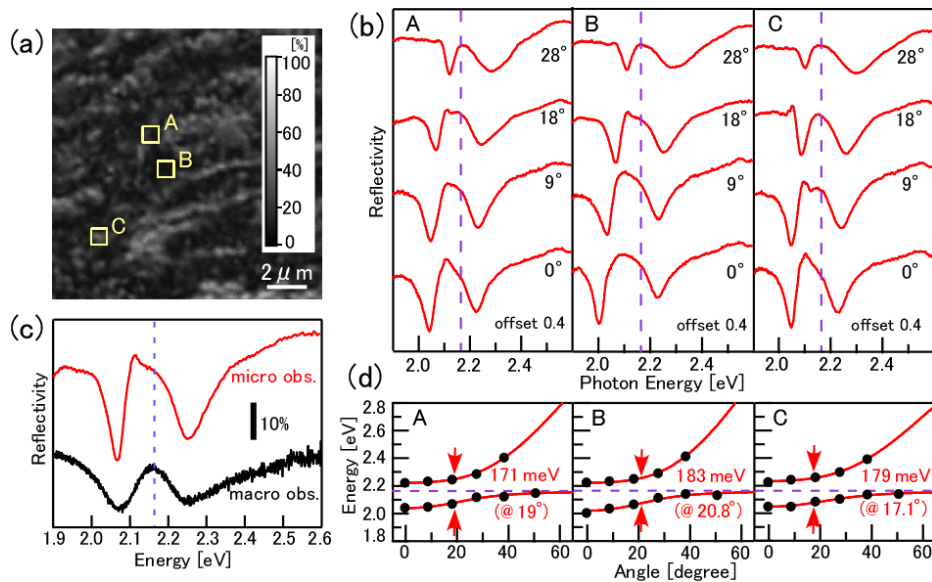

Fig. 4. (a) Microscopic reflection image of the organic microcavity at a 17 μm × 17 μm region (512 × 512 pixels). (b) Reflectivity of the microcavity at 0.8 μm × 0.8 μm areas (30 × 30 pixels) indicated by squares A, B and C in Fig. 4(a) as a function of viewing angle for s-polarized incident light. Viewing angles corresponding to the individual spectra are indicated on the right side. (c) Typical reflection spectra measured with microscopic and macroscopic systems. (d) Angular dependent energy dispersion of the upper and lower cavity polariton branches. The solid lines are the best fittings to the data.

some kind of inhomogeneous broadening in the macroscopic spectra is removed.

Circles in Figs. 4(d) -A, -B and -C show the dip energies in the corresponding spectra in Fig. 4(b) and solid lines are their fitted curves. The values of Ω at each location were evaluated as 171, 183 and 179 meV, respectively. Average value over the 17 μm × 17 μm image region (Fig 4(a)) was 180 meV, slightly less than 188 meV obtained by the macroscopic observation. It is, however, within the deviation of Ω, being estimated as ± 10 %.

Possible origins of the micrometer-scale spatial inhomogeneity in Ω are as follows. As discussed above, the value of Ω is determined by the factor of $(\alpha L_{active}/n_{eff}^2 L_{eff})^{1/2}$. As for L_{active} and L_{eff}, they are basically similar quantities and resemble each other. So their size distributions should also resemble each other. Thus, as is indicated by the expression of the factor, contributions of their fluctuations would cancel each other. Furthermore, the amount of deviations of L_{active} and L_{eff} should become smaller in microscopic region (ca. ± 5%). This may convince us that the parameters L_{active} and L_{eff} are less effective to the inhomogeneity of Ω. Remaining parameters α and n_{eff} are determined by J's local concentration in the active layer. They appear in the numerator and denominator in the factor, respectively, but they do in different orders. In addition, α is basically proportional to the J's concentration, and n_{eff} depends only slightly on the that as discussed in Fig. 3. So the contributions from their density fluctuations can not be cancelled out. Thus we conclude for the moment that the micrometer-scale inhomogeneity in Ω is mainly due to the spatial distribution of J's concentration in the film.

As for the micrometer-scale inhomogeneity in a reflectance image observed at a specific incident-light-angle (e.g. Fig. 4(a)), it is associated with not only the local distribution of J's concentration but also that of L_{active}. This is because the local fluctuation of L_{active} leads to that of the local resonance angle in our sample. Likewise, we consider the inhomogeneous broadening of the macro-spectra arise from both of the local distributions.

In summary, we fabricated planar metal-mirror microcavity containing high concentration PIC J-aggregates and characterized its specific optical properties. Large Rabi-splitting from 100 to 250 meV was obtained depending on the concentration of the PIC J-aggregates. It is presented that the Rabi-splitting is proportional to the factor of $(\alpha L_{active}/n_{eff}^2 L_{eff})^{1/2}$. We also presented microscopic reflection properties of the microcavities with our improved microscope. We found there is a micrometer-scale spatial inhomogeneity in the Rabi-splitting. One possible origin of this inhomogeneity is a spatial distribution of J's concentration in the active layer.

Acknowledgements

References

[1] M. S. Skolnick, T. A. Fisher, and D. M. Whittaker, Semicond. Sci. Technol. 13, 645 (1998).
[2] J. McKeever, A. Boca, A. D. Boozer, J. R. Buck, and H. J. Kimble, Nature, 425, 268 (2003).
[3] J. R. Tischler, M. S. Bradley, V. Bulovic, J. H. Song, and A. Nurmikko, Phys. Rev. Lett. 95, 036401 (2005).
[4] C. Ciuti, Phys. Rev. Lett. 69, 245304 (2004).
[5] H. Ajiki and H. Ishihara, J. Phys. Soc. Jpn. 76, 053401, (2007).
[6] D. G. Lidzey, D. D. C. Bradley, M. S. Skolnick, T. Virgili, S. Walker, and D. M. Whittaker, Nature 395, 53 (1998).
[7] L. G. Connolly, D. G. Lidzey, R. Butté, A. M. Adawi, D. M. Whittaker, M. S. Skolnick, and R. Airey, Appl. Phys. Lett. 83, 5377 (2003).
[8] R. J. Holmes and S. R. Forrest, Organic Electronics 8, 77 (2007).
[9] P. A. Hobson, W. L. Barnes, D. G. Lidzey, G. A. Gehring, D. M. Whittaker, M. S. Skolnick, and S. Walker, Appl. Phys. Lett. 81, 3519 (2002).
[10] M. Oda, K. Hirata, T. Inoue, Y. Obara, T. Fujimura, and T. Tani, Phys. Stat. Sol. (c) 6, 288 (2009).
[11] P. O. J. Schere, S. F. Fisher, Chem. Phys. 86 267 (1984).
[12] E. W. Knapp, Chem. Phys. 85 73 (1984).
[13] J. Knoester, J. Chem. Phys. 99 8466 (1993).
[14] V. Savona, L. C. Andreani, P. Schwendimann, A. Quattropani, Solid State Commun. 93 (1995) 733.